Stratospheric Transit Time Distributions Derived from Satellite Water Vapor Measurements

William J. Randel[1], Aurélien Podglajen[2], and Fei Wu[3]

[1]National Center for Atmospheric Research (UCAR)
[2]Laboratoire de météorologie dynamique, Ecole Polytechnique
[3]National Center for Atmospheric Research

May 21, 2024

Abstract

Stratospheric transit time distributions (age-of-air spectra) are estimated using satellite water vapor (H2O) measurements from the Microwave Limb Sounder over 2004-2021 assuming stationary transport. Latitude-altitude dependent spectra are derived from correlations of interannual H2O anomalies with respect to the tropical tropopause source region, fitted with an inverse Gaussian distribution function. The reconstructions accurately capture interannual H2O variability in the 'tropical pipe' and global lower stratosphere, regions of relatively fast transport (~1-2 years) in the Brewer-Dobson circulation. The calculations provide novel observational estimates of the corresponding 'short transit-time' part of the age spectrum in these regions, including the mode. However, the H2O results do not constrain the longer transit-time 'tail' of the age spectra, and the mean age of air and spectral widths are systematically underestimated compared to other data. We compare observational results with parallel calculations applied to the WACCM chemistry-climate model and the CLaMS chemistry-transport model, and additionally evaluate the method in CLaMS by comparing with spectra from idealized pulse tracers. Because the age spectra accurately capture H2O interannual variations originating from the tropical tropopause, they can be used to identify 'other' sources of variability in the lower stratosphere, and we use these calculations to quantify H2O anomalies in the Southern Hemisphere linked to the Australian New Years fires in early 2020 and the Hunga volcanic eruption in 2022.

Hosted file

`age spectra submitted.docx` available at https://authorea.com/users/536863/articles/939721-stratospheric-transit-time-distributions-derived-from-satellite-water-vapor-measurements

Stratospheric Transit Time Distributions Derived from Satellite Water Vapor Measurements

William J. Randel[1], Aurelien Podglajen[2], and Fei Wu[1]

[1] NSF National Center for Atmospheric Research, Boulder, CO 80307

[2] Laboratoire de Météorologie Dynamique (LMD/IPSL), École Normale Supérieure, CNRS, Paris, France

Corresponding author: William Randel (randel@ucar.edu)

Key Points:

- Stratospheric transit time distributions (age spectra) are derived from time series of satellite water vapor measurements
- Water vapor reconstructions from age spectra accurately capture variability in the tropics up to 30 km and in the global lower stratosphere
- Age spectrum results are compared between observations and global model simulations

Abstract

Stratospheric transit time distributions (age-of-air spectra) are estimated using satellite water vapor (H_2O) measurements from the Microwave Limb Sounder over 2004-2021 assuming stationary transport. Latitude-altitude dependent spectra are derived from correlations of interannual H_2O anomalies with respect to the tropical tropopause source region, fitted with an inverse Gaussian distribution function. The reconstructions accurately capture interannual H_2O variability in the 'tropical pipe' and global lower stratosphere, regions of relatively fast transport (~1-2 years) in the Brewer-Dobson circulation. The calculations provide novel observational estimates of the corresponding 'short transit-time' part of the age spectrum in these regions, including the mode. However, the H_2O results do not constrain the longer transit-time 'tail' of the age spectra, and the mean age of air and spectral widths are systematically underestimated compared to other data. We compare observational results with parallel calculations applied to the WACCM chemistry-climate model and the CLaMS chemistry-transport model, and additionally evaluate the method in CLaMS by comparing with spectra from idealized pulse tracers. Because the age spectra accurately capture H_2O interannual variations originating from the tropical tropopause, they can be used to identify 'other' sources of variability in the lower stratosphere, and we use these calculations to quantify H_2O anomalies in the Southern Hemisphere linked to the Australian New Years fires in early 2020 and the Hunga volcanic eruption in 2022.

Plain Language Summary

Stratospheric water vapor (H_2O) is mainly controlled by transport across the cold tropical tropopause, which sets the entry value for the global stratosphere. Interannual variations in H_2O originate near the tropical tropopause and then propagate throughout the stratosphere with the global Brewer-Dobson circulation (BDC), where anomalies are lagged in time and smoothed by mixing. We use the observed time series of H_2O from the Microwave Limb Sounder during 2004-2021 to calculate transit time distributions (also called age spectra) from the tropical tropopause source region, based on fits to an idealized inverse Gaussian distribution. The results accurately capture H_2O variability in the tropics up to 30 km and in the global lower stratosphere, regions of relatively fast transport (~1-2 years) in the BDC. The calculations provide novel observational estimates of the short transit time part of the age spectra in these regions, although the longer transit time part of the spectra are poorly constrained. The calculations are straightforward to apply to global models, and we compare observational results with simulations from the WACCM and CLaMS models.

1 Introduction

The stratospheric age spectrum is the probability distribution of transit times from the stratospheric entry point (i.e., the tropical tropopause) to any location, and thus links the boundary sources of transported constituents with their global distribution (Kida, 1983; Hall and Plumb, 1994). It provides a powerful diagnostic of the effective stratospheric circulation and is especially useful for evaluating model transport behavior (e.g., Hall et al, 1999; Waugh and Hall, 2002). The age spectrum can be computed explicitly with a numerical model using pulse tracers (e.g., Hall and Plumb, 1994), and recent work has focused on evaluating the detailed seasonal and interannual variability of model transport (Li et al, 2012, Ploeger and Birner, 2016; Ploeger et al, 2021). Model spectra have also been deduced using a set of chemically active trace species, either in idealized set-ups (Podglajen and Ploeger, 2019; Hauck et al, 2019) or observations (Schoeberl et al, 2005; Hauck et al, 2020). Stratospheric age spectra have also been derived from trajectory calculations using three-dimensional wind fields from meteorological analyses or reanalyses (Schoeberl et al, 2003; Diallo et al, 2012), and large differences in results demonstrate the uncertainty related to reanalyses (Ploeger et al, 2019), in particular their representation of heating rates.

A related quantity is the mean age of air (the first moment of the age spectrum) which can be exactly diagnosed using idealized linearly increasing conservative tracers (Hall and Plumb, 1994). While the mean age is a useful metric for comparison to observations, using for example measurements of carbon dioxide (CO_2) and sulfur hexafluoride (SF_6) (Waugh and Hall, 2002), it provides much less information than the full age spectrum.

While the stratospheric age spectrum is a common diagnostic for models, it cannot be measured directly from observations. Rather, observational estimates have been made using conservative tracers such as carbon dioxide (CO_2; Andrews et al, 1999; 2001) or combinations of tracers with varying photochemical lifetimes (Schoeberl et al, 2005; Hauck et al, 2020). These calculations assume an idealized functional form for the age spectrum (often taken to be an inverse Gaussian, as discussed below) and optimize a fit to the observed constituent measurements. Johnson et al (1999) used a combination of satellite and balloon-borne measurements of water vapor (H_2O) and methane (CH_4) to estimate age spectra, calculating the spectra by direct Fourier inversion and singular value decomposition. Our work revisits the estimation of stratospheric age spectra using the long-term (2004-2021) global measurements of H_2O from the Aura Microwave Limb Sounder (MLS) instrument. We analyze time series of observations at the tropical tropopause source region and throughout the global stratosphere, and derive age spectra from optimal correlations using an idealized inverse Gaussian functional form. In additional to observational results we perform parallel analyses on chemistry-climate model simulations to test the methodology, inform the data analysis and evaluate the model behavior.

Because the age spectrum reconstruction can accurately capture H_2O variability tied to the tropical tropopause, differences with observations can be used to identify additional sources of H_2O. We demonstrate these calculations to quantify H_2O input to the Southern Hemisphere lower stratosphere from the Australian New Years fires in early 2020 and the Hunga volcanic eruption in 2022.

2. Observations and model simulations

2.1 MLS data

We analyze water vapor measurements from the Aura MLS instrument (Read et al, 2007) covering the period September 2004 – March 2021, using retrieval version 5.1 (Livesey et al, 2020). Data are available for standard pressure levels (12 per decade) for levels 316 to above 1 hPa, with a vertical resolution of ~3 km. The precision of MLS H_2O over 100-1 hPa is 5-7% for a single profile and 20 times smaller for monthly zonal means. The MLS v5 H_2O retrievals have corrected a small positive drift found in previous v4 results (Livesey et al, 2021). The age spectra are calculated using data prior to the Hunga volcanic eruption in January 2022, which injected a large amount of H_2O into the stratosphere (Millan et al, 2022), and our results are not influenced by that event. We include some updated MLS results through early 2024 in Section 4b. Our analyses are based on monthly and zonally averaged data on a 5^o latitude grid, which have been deseasonalized with respect to the long-term monthly seasonal cycle. We use deseasonalized data because we are interested in quantifying the behavior of interannual variations in H_2O, but we note that very similar age spectrum results are found if the seasonal cycle is included.

2.2 Global models

We perform parallel analyses deriving age spectra from global model simulations to both inform the observational data studies and evaluate model transport. We use output from the Whole Atmosphere Community Climate Model (WACCM), which is a comprehensive chemistry climate model that spans the altitude range from the surface to ~140 km; WACCM details are described at https://www2.acom.ucar.edu/gcm/waccm. The results here are derived from the recently updated version 6 (WACCM6) described in Gettelman et al (2019). Our analyses use standard historical simulations from WACCM spanning the years 1960-2014, using horizontal resolution 2 x 2 degrees and 70 vertical levels (vertical resolution ~1 km in the stratosphere), and the quasi-biennial oscillation (QBO) in these runs was nudged to observations. We analyze deseasonalized monthly and zonal average fields of H_2O, and we note that this model includes methane (CH_4) oxidation effects on stratospheric H_2O.

We also analyze results derived from the Chemical Lagrangian Model of the Stratosphere (CLaMS), which has been used extensively for stratospheric age-of-air calculations (Ploeger and Birner, 2016; Podglajen and Ploeger, 2019). The model is driven by ERA-interim (Dee et al., 2011) wind and heating rates and features a dedicated parameterisation of small-scale mixing (Konopka et al., 2004). CLaMS also includes CH_4 oxidation effects on stratospheric H_2O. The model set-up used here is described by Pommrich et al. (2014) and includes additional pulse tracers (Ploeger and Birner, 2016) released at the tropical tropopause with a 2-month resolution along the transit-time axis extending up to 10 years.

3 Results

3.1 Deriving age spectra from time series of H_2O

Aura MLS provides a long-term (more than 17 years) global observational data record of stratospheric water vapor (H_2O), which has been used extensively in empirical data studies and model evaluations (e.g. Kawatani et al, 2014; Diallo et al, 2018; Yu et al, 2022). It is well-known that H_2O in the lower and middle stratosphere is mainly controlled by the tropical cold point temperature, while CH_4 oxidation contributes to (low frequency) H_2O variations in regions of 'older' stratospheric air (e.g. Yu et al., 2022; Tao et al., 2023). The MLS data show that stratospheric H_2O anomalies originate near the tropical tropopause and propagate coherently in latitude and height throughout the stratosphere, transported by the Brewer-Dobson circulation (Randel and Park, 2019). During such transport, the H_2O anomalies are lagged in time and systematically reduced in amplitude compared to variations at the tropical tropopause source region, due to advection and mixing. This is the fundamental signature of the vertical propagation of H_2O over the equator, the so-called tape recorder signal (Mote et al, 1996) found both in seasonal cycle and interannual H_2O anomalies. This behavior in the deseasonalized MLS H_2O data in the tropics is illustrated in Fig. 1a, which shows time series of anomalies at the tropopause source region (83 hPa), and at levels 46 hPa and 18 hPa, for data averaged over 10^o

N-S. As a note, the 83 hPa H_2O anomalies closely follow corresponding variations in cold point tropopause temperature, with correlations close to 0.9 (Randel and Park, 2019). The H_2O anomalies at upper levels are lagged in time, smoothed and reduced in amplitude compared to the variations at 83 hPa. Similar behavior is found for H_2O anomalies that propagate meridionally to the extratropical lower stratosphere in both hemispheres (Randel and Park, 2019).

As reviewed by Waugh and Hall (2002), the age spectrum mathematical problem is defined in a straightforward manner as:

$$X_B(t) = \int X_A(t-\tau) * G(\tau) d\tau \qquad (1)$$

Here $X_A(t)$ represents the source function of H_2O for air entering the stratosphere near the tropical tropopause (83 hPa tropical H_2O anomalies in this case, the lower level curve in Fig. 1b), $X_B(t)$ is the H_2O at some 'distant' location in the stratosphere, and $G(\tau)$ is the age-of-air spectrum. We note that this expression is only valid for stationary transport, where $G(\tau)$ does not depend on time. $G(\tau)$ is often characterized by an inverse Gaussian distribution of the form:

$$G_{\Gamma,\Delta}(\tau) = \sqrt{\frac{\Gamma^3}{4\pi\Delta^2\tau^3}}\, exp\left(\frac{-\Gamma(\tau-\Gamma)^2}{4\Delta^2\tau}\right) \qquad (2)$$

with parameters Γ=mean age and Δ=spectral width (Waugh and Hall, 2002). The mode (most likely value) is given by:

$$M_{\Gamma,\Delta} = \Gamma\left[\sqrt{(1+9\frac{\Delta^4}{\Gamma^4})} - 3\frac{\Delta^2}{\Gamma^2}\right] \qquad (3)$$

This $G_{\Gamma,\Delta}(\tau)$ is based on the solution to a 1-dimensional diffusive transport problem (Hall and Plumb, 1994). Our calculations involve deriving empirical estimates of $G_{\Gamma,\Delta}(\tau)$ in Eqns. 1-2 by finding optimal correlations between observed H_2O time series and $X_B(t)$ derived from Eq. 1, to obtain the best-fit age spectrum $G_{\Gamma,\Delta}(\tau)$. We note that our calculations provide a different and complementary technique to the Fourier inversion or singular value decomposition calculations used by Johnson et al (1999).

Our calculations use the monthly time series of MLS data over September 2004 – March 2021 (~16.5 years), and we derive the convolution in Eq. 1 using a $G(\tau)$ window of width 36 months, which reduces the length of $X_B(t)$ to ~13.5 years (September 2007-March 2021). The choice of 36-month convolution width in Eq. 1 is made to balance resolution of $G_{\Gamma,\Delta}(\tau)$ vs. the length of the available data record, and hence focuses on the short time scale structure of the age spectrum rather than on the tail of the distribution; this is an important detail discussed further below. Tests using a longer window (e.g., 60 months) do not show significant differences from the results shown here.

We demonstrate these calculations for the MLS H_2O time series at the equator and 18 hPa shown in Fig. 1a. Figure 1b shows the correlation between calculated $X_B(t)$ and observed $H_2O(t)$ as a function of the parameters Γ and Δ in Eq. 2, and the results identify an absolute maximum in the correlation for Γ=18 months and Δ=3 months. Figure 1c shows this derived age spectrum with a peak (modal) value of 16 months. The resulting time series of $X_B(t)$ at 18 hPa is shown as the red line in Fig. 1a, which has a correlation of 0.83 with the observed H_2O; corresponding results are also shown for the 46 hPa level in Fig. 1a. At all levels throughout the tropics the H_2O correlations exhibit maximum values similar to Fig. 1b that are used to select optimal Γ and Δ fit parameters. However, we note that the correlation maxima in Fig. 1b are somewhat broad in (Γ,Δ) space with highest values maximizing along a line with constant mode M (heavy dashed line in Fig. 1b), and relatively strong H_2O correlations occur for very different (Γ,Δ) combinations. We find that this is a general result of these parameter sweep calculations. As a note, estimates of best fit Γ and Δ based on minimum rms differences of (calculated $X_B(t)$ minus observed $H_2O(t)$) give very similar results to those for maximum correlation.

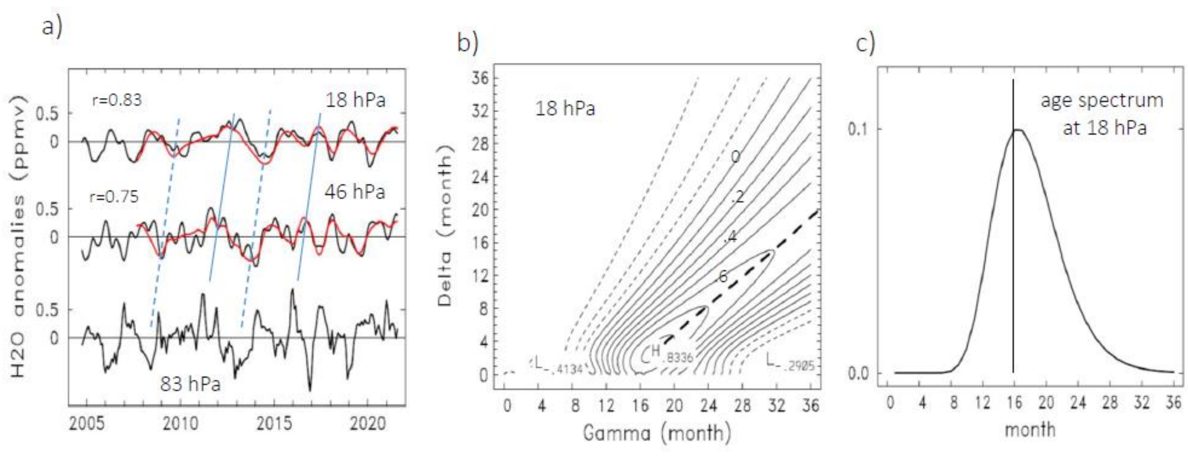

Figure 1. (a) Black lines show time series of tropical (10^o N-S) MLS H_2O deseasonalized anomalies at 83 hPa (source region near tropical tropical tropopause), 46 and 18 hPa.

Red lines at 46 and 18 hPa show $X_B(t)$ reconstructions based on convolving the 83 hPa time series with derived age spectra. Solid and dashed blue lines trace several maxima and minima in altitude. (b) Correlation of observed $H_2O(t)$ at 18 hPa vs. the age spectrum reconstruction $X_B(t)$ as a function of the parameters (Γ, Δ), with a maximum at (18,3). The heavy dashed line corresponds to a constant mode M that crosses through the maximum correlation point, M=16 months in this case. (c) Resulting optimum age spectrum at 18 hPa.

These calculations can be repeated at each latitude and height, and Fig. 2a shows the resulting age spectra derived from MLS H_2O data in the tropics over 68-10 hPa (~19-32 km). The modal (most likely) values trace the phase speed of vertical propagation in the H_2O tape recorder, and this calculation provides novel quantification of this speed as a complement to simple lag correlations e.g. Niwano et al, 2003; Glanville and Birner, 2017. The width of the age spectra broadens with altitude in Fig. 2a, indicative of increased mixing of air between the tropics and extratropics at higher levels.

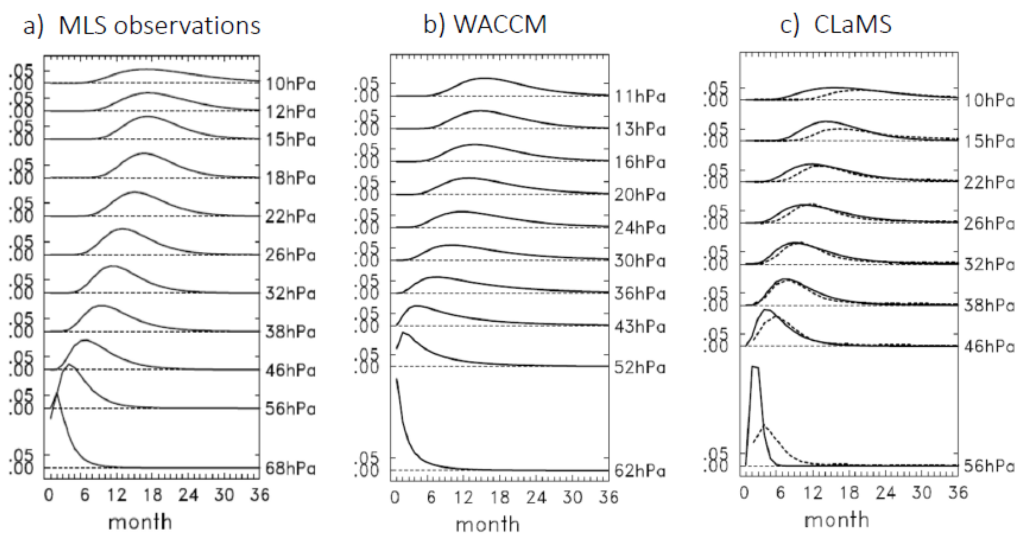

Figure 2. Tropical (10^o N-S) age spectra versus altitude (pressure level) derived from H_2O time series, for (a) MLS observations, (b) WACCM and (c) CLaMS model. Dashed lines in (c) show age spectra derived from the CLaMS pulse tracers.

3.2 Comparisons with WACCM and CLaMS model calculations

The calculations described above are easy to implement using standard monthly mean output of chemistry-climate model simulations. For both the WACCM and CLaMS model calculations, we identify a source time series of H_2O near the model tropical tropopause, which is at p=87 hPa in WACCM and p=82 hPa in CLaMS, and the rest of the calculations proceed as above. Tropical age-of-air spectra derived from WACCM and CLaMS model simulations of H_2O are shown in Figs. 2b-c, showing approximate agreement with MLS results (Fig. 2a) in terms of modal times and spectral width. This is consistent with the good performances of WACCM and ClaMS models to simulate atmospheric water vapor variability (Gettelman et al, 2019; Yu et al., 2022; Diallo et al., 2018; Kopopka et al., 2022; Tao et al., 2023). Direct comparison of the calculated spectra at several levels in the tropics (10^o N-S) are shown in Fig. 3. The comparisons show approximate agreement in the shape of the spectra, and that inferred vertical propagation times (spectral mode) are slightly faster in both models compared to MLS observations. These WACCM6 results are consistent with the H_2O tape recorder comparisons to MLS data shown in Gettelman et al, 2019.

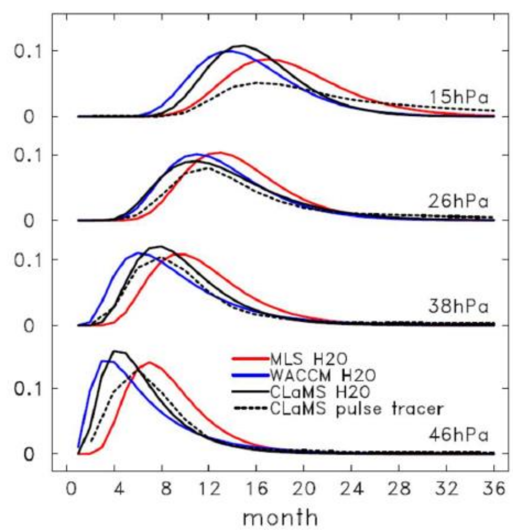

Figure 3. Comparison of tropical (10^o N-S) age spectra derived from H_2O time series at several pressure levels, from MLS observations, WACCM and CLaMS models. Dashed black lines show corresponding results from the CLaMS pulse tracers.

3.3 Comparing CLaMS spectra from H_2O with results from pulse tracers

For the CLaMS simulations analyzed here we can directly compare the age-of-air spectra derived from H_2O with model calculations based on pulse tracers, as described in Ploeger and Birner (2016). Figures 2c and 3 include direct comparisons of the tropical age spectra between the two calculations, and Fig. 4 compares tropical vertical profiles of derived age, width and mode. The spectra show reasonable agreement with the H_2O fit results in the lower stratosphere (e.g. lower altitude or higher pressure levels in Fig. 3), including the mode estimate. Larger differences become evident at upper levels (15 and 10 hPa), where the pulse tracer calculations show spectra with larger components of aged air, i.e. a larger tail to the spectra.

Comparisons of the derived mean age and width from the pulse tracers show larger differences with the H_2O estimates (Figs. 4a-b). The tropical H_2O-derived ages from MLS, WACCM and CLaMS are similar in Fig. 4a, increasing with height to approximately 18-24 months near 10 hPa. However, these estimates are substantially smaller than the CLaMS pulse tracer values and also only about half as large as the tropical age-of-air profile derived from CO_2 and SF_6 observations in Waugh and Hall (2002). This difference can be explained by noting that the age is the first moment of the age spectrum and is sensitive to the longer time scales (tail) of the distribution. The longer tail of the pulse tracer spectra compared to the H_2O inverse Gaussian fits can be seen in Figs. 2-3. While the H_2O variations in the tropical pipe are quite accurately fit by the assumed inverse Gaussian distribution (with correlations of order 0.8, as shown in Fig. 1a), these fits mostly constrain the fast part of the spectrum (less than ~2 years) and less-so for the tail, which more strongly influences the age. In a similar manner, the spectral widths (second moment) of the pulse tracer spectra are much larger than the H_2O inverse Gaussian fits (Fig. 4b) due to the influence of the tail. Hence while our choice of an inverse Gaussian distribution accurately reproduces the ‘fast’ transport of H_2O from the tropical tropopause and gives accurate estimates of the mode (Fig. 4c), it provides a poor estimate for mean age and spectral width, which depend heavily on the tail of the spectrum.

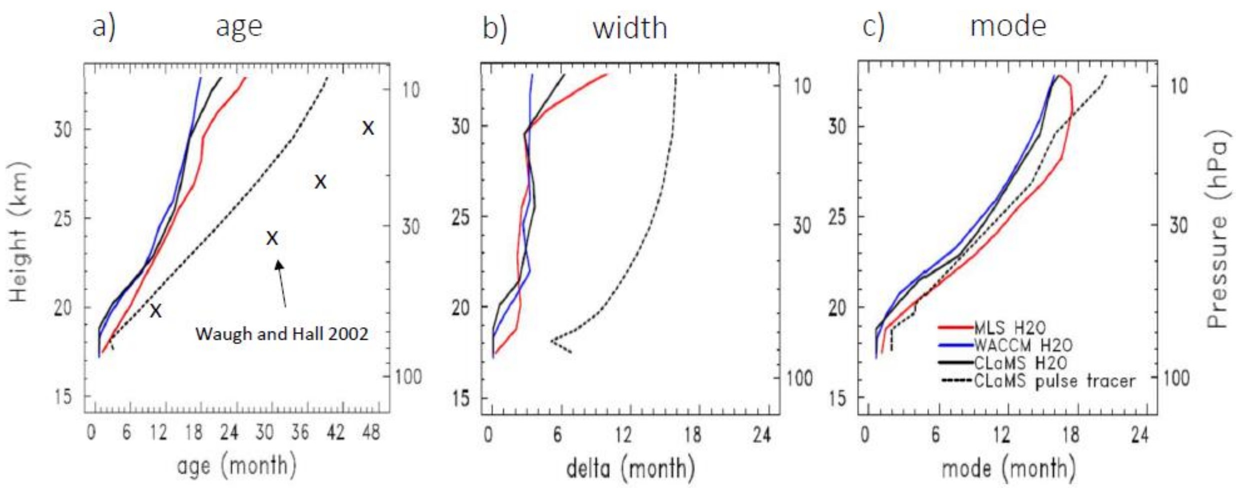

Figure 4. Vertical profiles of tropical (10° N-S) age spectrum parameters derived from the H_2O time series fits, for MLS observations, WACCM and CLaMS model results. The dashed black lines show corresponding results from the CLaMS pulse tracers. The age results in (a) also include values derived from CO_2 and SF_6 observations described in Waugh and Hall (2002).

3.4 Transit time distribution in the extratropical lower stratosphere

In addition to coherent vertical propagation in the tropical pipe, the MLS H_2O anomalies exhibit coherent quasi-isentropic horizontal transport from the tropics to the extratropical lower stratosphere of both hemispheres, with strong (lag) correlations (>0.7) on the time scale of a few months (e.g. Randel and Park, 2019). Our methodology can also be applied to deduce the age spectra associated with this transport pathway. Results of these calculations show that high $H_2O(t)$ vs. $X_B(t)$ correlations typically maximize along a broad 'ridge' in (Γ, Δ) space consistent with a constant mode, but without a strong correlation maximum as seen in the tropics (e.g. Fig. 1b). This behavior is illustrated in Fig. 5a, showing the age spectrum fit for H_2O anomalies at 48° N, 100hPa. Strong correlations are found along the ridge in (Γ,Δ) space corresponding to a constant mode M=2.5 months (heavy dashed line in Fig. 5a), with relatively small differences in the H_2O correlations along this line. In this case the maximum correlation (r=.908) is identified at point A (Γ=7, Δ=5) but nearly as high correlation (r=.895) is found at point B (Γ=26, Δ=36). Hence the specific (Γ,Δ) values and detailed shape of the spectra (Fig. 5b) are poorly constrained by these calculations, although very high H_2O anomaly correlations are derived in both cases

(Fig. 5c). This is typical behavior for age spectra fits in the extratropical lower stratosphere and cautions against over-interpreting details of the derived spectra.

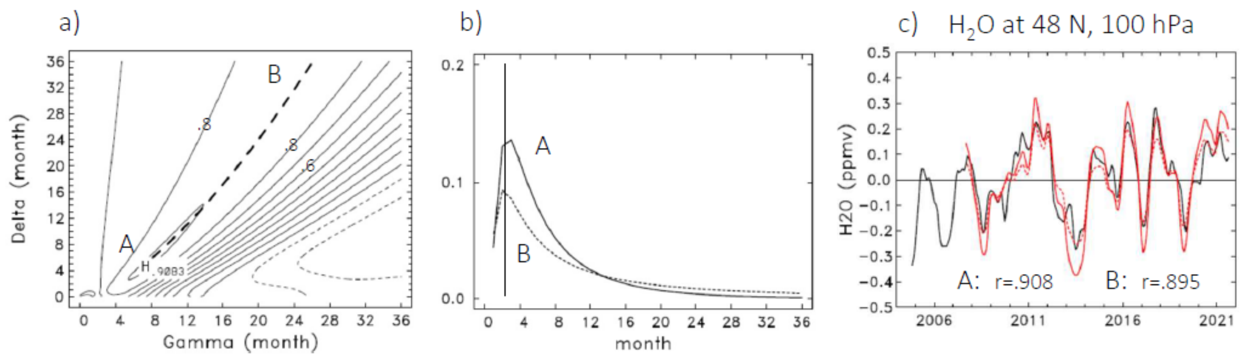

Figure 5. (a) Correlation of observed H_2O anomalies at 48^o N, 100 hPa with the age spectrum reconstruction $X_B(t)$ as a function of the parameters (Γ, Δ). Relatively high correlations are observed over the locus of points corresponding to a mode of 2.5 months, as noted by the thick dotted line spanning A to B. (b) Age spectra corresponding to points A and B. The mode for both spectra (2.5 months) are indicated by the vertical line. (c) Time series of observed H_2O anomalies (black) and $X_B(t)$ reconstructions using the respective A and B age spectra (solid and red dashed lines, respectively).

Figure 6 shown the calculated age spectra at 100 hPa for results at 45^o and 65^o N and S, from MLS H_2O along with the corresponding WACCM and CLaMS model results. The results show broad age spectra peaking at time scales of ~2-4 months, with the spectra shifting to longer modal times between 45^o and 65^o in both hemispheres. The WACCM calculations are in reasonable agreement with MLS results, while CLaMS H_2O spectra hint at systematically shorter modal times, possibly suggesting faster quasi-horizontal transports in CLaMS.

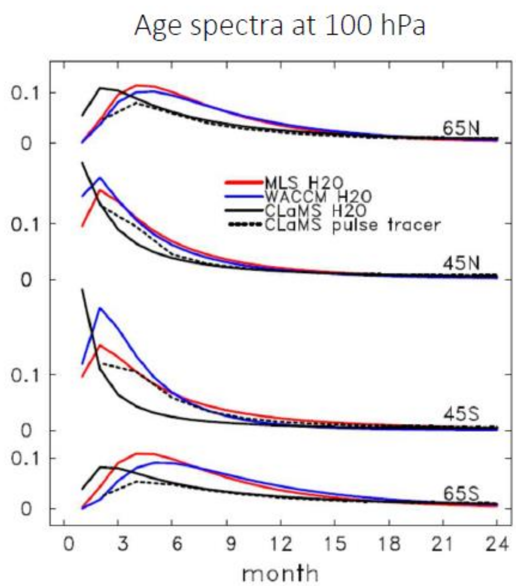

Figure 6. 100 hPa age spectra derived from H_2O time series at 45^o and 65^o N and S, showing latitude dependent structure associated with quasi-horizontal transport from the tropics to extratropics. Dashed black lines show corresponding results derived from the CLaMS pulse tracers.

3.5 Global behavior

One measure of the goodness-of-fit of $G_{\Gamma,\Delta}(\tau)$ is how well the calculated $X_B(t)$ agrees with observed $H_2O(t)$. Figure 7a shows this correlation as a function of latitude and height derived from the MLS H_2O data, showing high correlations (>0.7) extending upwards in the tropics to ~32 km and throughout the global lower stratosphere. These are the regions of strong interannual variability in H_2O controlled by relatively rapid transport from the tropical tropopause region. Note that strong lower stratosphere correlations extend all the way to the pole in the NH in Fig. 7a, while they only extend to ~60^o S in the SH. This is because local dehydration in the Antarctic polar vortex in winter effectively decouples polar H_2O from the tropical tropopause. The high correlations in Fig. 7a demonstrate accurate fits of the observed interannual variability using age spectra derived from the MLS H_2O measurements. In regions of low correlations, e.g. the extratropical middle stratosphere and above 10 hPa, the H_2O data alone are not as useful for constraining the transit time distribution.

Parallel results derived from WACCM and CLaMS H_2O fields are shown in Fig. 7b-c. WACCM results are similar to MLS statistics (Fig. 7a) both in terms of magnitude and spatial patterns. The correlations from WACCM are smoother compared to the observational results because we use a much longer time series from the model (~50 years) to evaluate the fits (compared to 16.5 years of data for MLS). The CLaMS age spectrum correlations (Fig. 7c) show patterns similar to MLS and WACCM, but the high correlations in the tropical pipe show weaker latitudinal gradients extending into middle latitudes, i.e. the tropical pipe appears less isolated in CLaMS compared to MLS and WACCM. This could be consistent with the faster meridional propagation time scales for CLaMS discussed above, or perhaps with a weaker subsidence/overturning circulation in midlatitudes.

For comparison, Figs. 7d-f show H_2O anomaly correlation patterns using simple lag regressions with respect to the tropical tropopause source region (picking the optimal time lag at each latitude and height). Results show patterns like the age spectra correlations (Figs. 7a-c), but the age spectrum systematically enhances the strongest correlations by ~0.1 to 0.2.

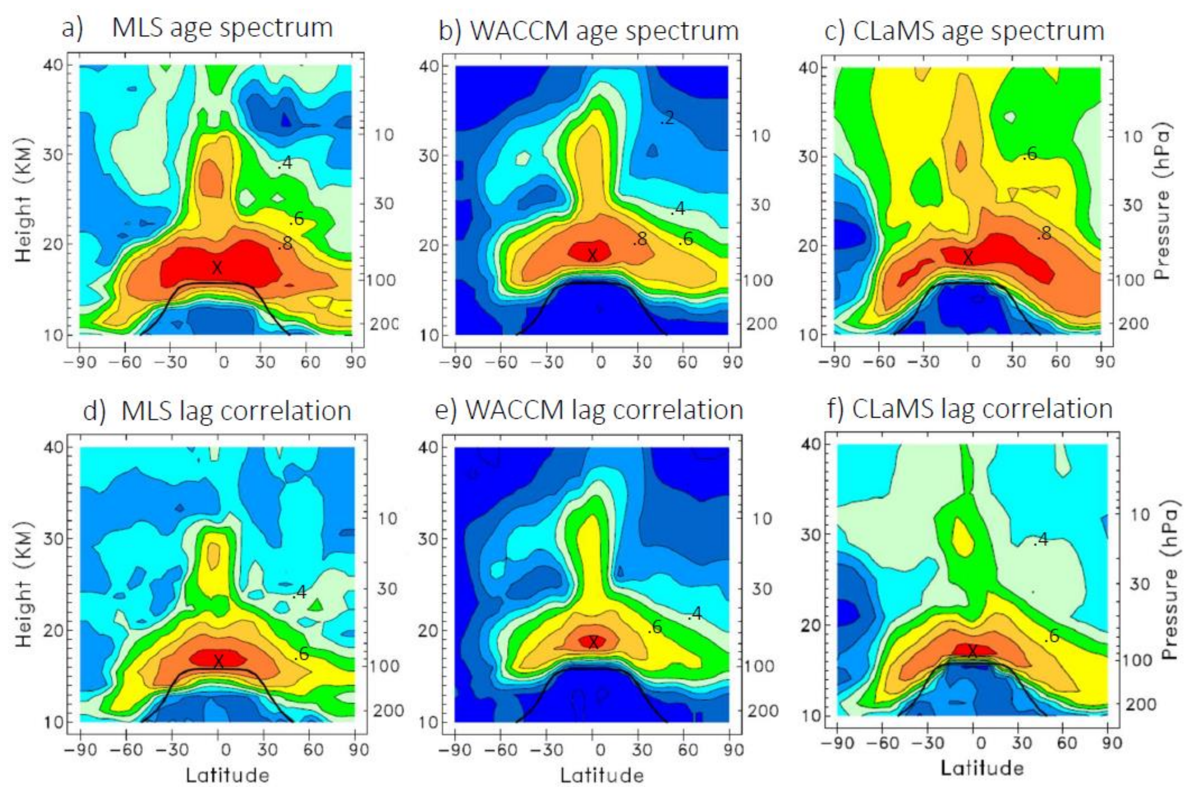

Figure 7. Correlations of observed H_2O time series versus reconstruction from derived age spectra for (a) MLS observations, (b) WACCM model and (c) CLaMS model. The ‘X’s denote the corresponding source regions at the tropical tropopause. Panels (d-f) show the corresponding results for simple lag correlations with respect to the tropical tropopause.

4. Discussion

4.1 Effects of CH_4 oxidation

CH_4 oxidation contributes to low-frequency H_2O variability in regions of 'older' stratospheric air, i.e., the extratropics of the middle stratosphere and in the tropics above ~30 km (Yu et al., 2023; Tao et al, 2023). However, CH_4 oxidation contributes little to H_2O fast variability in the tropical pipe and global lower stratosphere, although presumably the in-mixing of aged air (Neu and Plumb, 1999) is partly responsible for the reduction in H_2O correlations with altitude in the tropical pipe (and lack of correlations above ~30 km). Tests with WACCM of parallel calculations using the conserved quantity ($H_2O + 2*CH_4$) show only marginal increases in correlation and almost no changes in derived spectra compared to H_2O alone.

4.2 Identifying H_2O variability not linked to the tropical tropopause

Because so much of the interannual variability of H_2O in the lower stratosphere is captured by the age spectrum reconstruction (Fig. 7), it is interesting to examine the differences between observed vs. reconstructed anomalies to identify sources of variability not linked to transport from the tropical tropopause. Figure 8 compares the observed latitude vs. time evolution of MLS H_2O anomalies at 83 hPa (Fig. 8a) with the age spectrum reconstruction (Fig. 8b), and their differences (or residuals) shown in Fig. 8c. Here we have included MLS observations through March 2024, although the reconstructions are based on age spectra calculated with data prior to 2022. The H_2O anomalies in Fig. 8a show episodic maxima near the equator that propagate to extratropics, and there are persistent positive anomalies after 2020 linked to warm tropopause temperatures. As expected, the reconstruction (Fig. 8b) captures most of the H_2O variability and the residuals (Fig. 8c) are generally small (~0.1 ppmv). There are generally positive H_2O residuals over extratropics for the latter half of the record, which might reflect effects of CH_4 increases (in aged air) over time. However, somewhat larger residuals are observed for several specific periods in Fig. 8c. A localized maximum is seen in the SH low-to-middle latitudes during the first half of 2020, and these are likely related to H_2O injected into the lower stratosphere from the extreme Australian New Year (ANY) fires (Khaykin et al., 2020; Yu et al, 2021; Peterson et al, 2021; Friberg et al, 2023). Figure 9a shows a latitude vs. height cross section of the H_2O residuals for February 2020 showing positive anomalies up to 0.3 ppmv covering altitudes ~15-19 km over ~10-60^o S, and this region approximately overlaps the observed aerosol enhancement from the ANY fires (Rieger et al, 2021). Similar patterns of H_2O residuals are evident for the first 6 months of 2020, slowly declining in magnitude over time. While these are relatively small H_2O amounts (~0.1 to 0.3 ppmv), their temporal and spatial structure is strongly suggestive of links to the ANY fires.

Large and persistent H_2O residuals are also seen in Fig. 8c over SH high latitudes in late 2023, which are likely related to downward transport of H_2O from the Hunga volcanic eruption in early 2022 (Millan et al, 2022). While much of the Hunga H_2O plume was transported into the tropics above 25 km and upwards in the Brewer-Dobson circulation (Zhou et al, 2024), the global stratospheric circulation is expected to result in long-term downward transport over high latitudes. Figure 9b shows a cross-section of H_2O residuals in October 2023, highlighting large positive anomalies in middle and high latitudes of both hemispheres, reflecting the global transport of the plume nearly 2 years after the eruption. The SH high latitude maxima at lower levels in late 2023 may reflect the climatological enhanced downward transport in the lower stratosphere during SH winter and spring, and we note that there are positive H_2O residuals at high latitude in the NH during winters 2022-23 and 2023-24 in Fig. 8c that could likewise reflect the seasonal downward transport of Hunga H_2O anomalies. It is likely that these high latitude effects will continue and increase over time as the Hunga H_2O plume is transported downwards in the global stratospheric circulation.

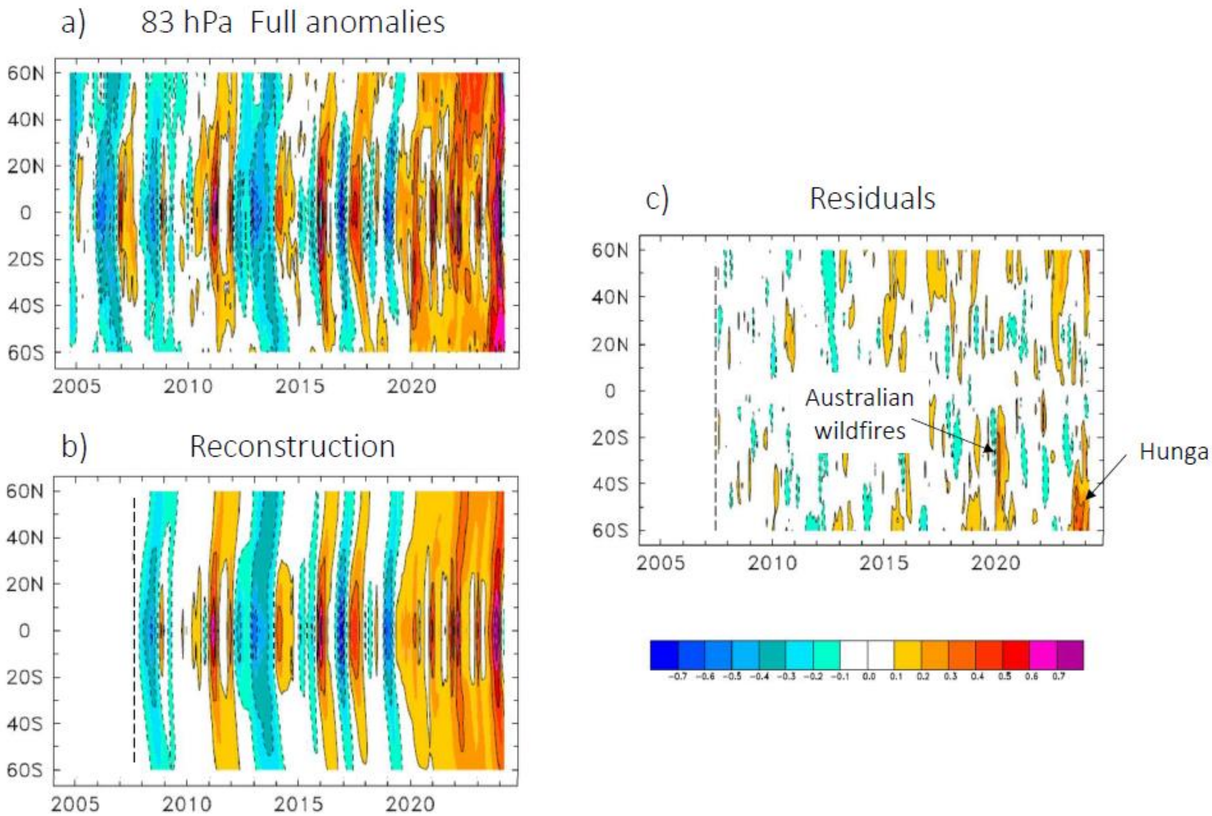

Figure 8. (a) Latitude vs. time section of deseasonalized MLS H_2O anomalies at 83 hPa. (b) Corresponding H_2O anomalies based on age spectrum reconstruction covering the period after September 2007. (c) Differences or residuals between observed and age spectrum reconstruction.

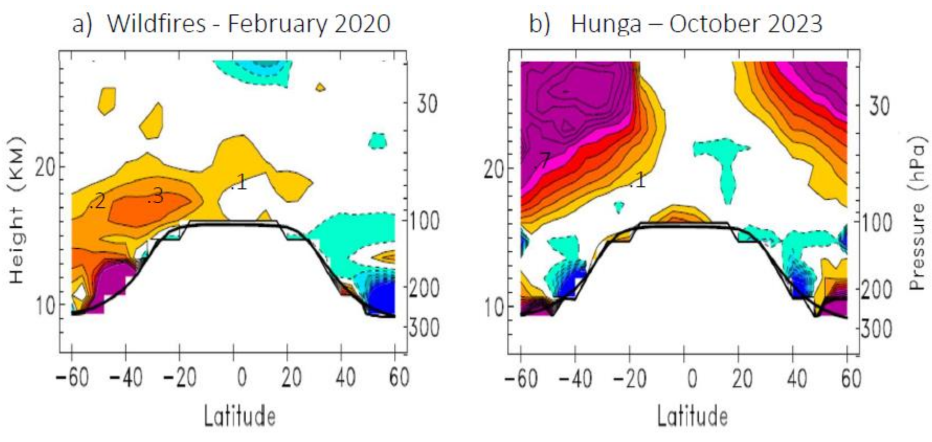

Figure 9. Height vs. latitude structure of H_2O residuals (ppmv) in (a) February 2020 and (b) October 2023 derived from differences between observed H_2O and age spectrum reconstruction.

5 Conclusions

We have used observed interannual variations in H_2O from MLS satellite observations to derive empirical stratospheric transit time distributions, based on optimal fits to an inverse Gaussian distribution function. These calculations are straightforward to apply to observational data or global model output. The results accurately capture H_2O interannual variability in the tropical pipe and global lower stratosphere (with anomaly correlations > 0.8 in Fig. 7), which are regions of relatively fast transport (~1-2 years) in the Brewer-Dobson circulation. These calculations provide novel estimates of the corresponding 'fast' part of the transit time distribution in these regions, including the mode, and the age spectrum reconstructions capture H_2O interannual variability more accurately than simple lag correlations. There is less information content for constraining the lower frequency tail of the age spectra, and the derived mean age and spectral width in the H_2O calculations are too low compared to other observational data. Parallel H_2O age spectra calculations from WACCM and CLaMS give similar results, and comparisons show faster upward transport in the tropics in the models compared to MLS data. Direct comparisons with spectra from CLaMS pulse tracers show reasonable agreement to the H_2O calculations in the lower stratosphere, while there are larger differences in the tropics above ~25 km where the pulse tracers give flatter age spectra with a wider tail (c.f. Fig. 2c). This corresponds to more in-mixing of aged air at the top of the tropical pipe, which is not captured in the H_2O results.

Because the age spectra reconstruction captures much of the H_2O transport from the tropical tropopause in the lower stratosphere (outside of the Antarctic vortex), differences with observations can identify additional sources of H_2O. We have demonstrated these calculations and identify anomalous H_2O in the SH lower stratosphere in early 2020 that appears linked to the ANY fires, as suggested by space-time overlap with observed ANY aerosols. The associated ANY H_2O anomalies are of order 0.1-0.3 ppmv (Fig. 9a) and persist for approximately 6 months. We additionally find persistent positive residuals over high SH latitudes in 2023 that are linked to the Hunga volcanic eruption in 2022. Quantification of these small anomalies is facilitated by the accurate fit of the background H_2O variability (transport from the tropical tropopause) using the empirically derived transit time distributions.

Acknowledgments

This work was motivated by discussions with Alan Plumb several years ago. We thank Rolando Garcia for discussions and critical comments on the manuscript. This work was partially supported under NASA Grant 80NSSC20K0928. The National Center for Atmospheric Research is supported by the US National Science Foundation.

Open Research

MLS satellite data were obtained from the Goddard Earth Sciences Data and Information Services Center at doi.org/10.5067/Aura/MLS/ CESM2/WACCM6 is an open-source community model, which was developed with support primarily from the National Science Foundation. See Gettelman et al. (2019). The CLaMS code used for the simulations in this article is available on the GitLab server: https://jugit.fz-juelich.de/clams/CLaMS (last access: 14 May 2024). ERA-Interim reanalysis data are available from the European Centre for Medium-Range Weather Forecasts (via https://apps.ecmwf.int/archive-catalogue/?class=ei, last access: 15 May 2021).

References

Andrews, A. E., K. A. Boering, B. C. Daube, and S. C. Wofsy (1999). Empirical age spectra from observations of stratospheric CO_2: Mean ages, vertical ascent rates, and dispersion in the lower tropical stratosphere, *J. Geophys. Res.*, *104*, 26,581–26,595.

Andrews, A. E., et al. (2001). Empirical age spectra for the midlatitude lower stratosphere from in situ observations of CO_2: Quantitative evidence for a subtropical “barrier” to horizontal transport, *J. Geophys. Res.*, *106*, 10,257–10,274.

Dee, D. P., and coauthors (2011). The ERA-Interim reanalysis: configuration and performance of the data assimilation system, Q. J. Roy. Meteor. Soc., 137, 553–597, https://doi.org/10.1002/qj.828, 2011.

Diallo, M., Legras, B., and Chédin, A. (2012). Age of stratospheric air in the ERA-Interim, Atmos. Chem. Phys., 12, 12133–12154, https://doi.org/10.5194/acp-12-12133-2012.

Diallo, M., Riese, M., Birner, T., Konopka, P., Müller, R., Hegglin, M. I., Santee, M. L., Baldwin, M., Legras, B., and Ploeger, F. (2018). Response of stratospheric water vapor and ozone to the unusual timing of El Niño and the QBO disruption in 2015–2016, Atmos. Chem. Phys., 18, 13055–13073, https://doi.org/10.5194/acp-18-13055-2018

Friberg, J., Martinsson, B. G., and Sporre, M. K.: Short- and long-term stratospheric impact of smoke from the 2019–2020 Australian wildfires (2023). Atmos. Chem. Phys., 23, 12557–12570, https://doi.org/10.5194/acp-23-12557-2023

Gettelman, A, and coauthors, (2019). "The Whole Atmosphere Community Climate Model Version 6 (WACCM6)." *Journal of Geophysical Research: Atmospheres* https://doi.org/10.1029/2019JD030943

Glanville, A. A. and Birner, T. (2017). Role of vertical and horizontal mixing in the tape recorder signal near the tropical tropopause, *Atmospheric Cemistry and Physics*, 17, 4337–4353, https://doi.org/10.5194/acp-17-4337-2017

Hall, T. M., and R. A. Plumb (1994). Age as a diagnostic of stratospheric transport, *J. Geophys. Res.*, *99*, 1059–1070.

Hall, T. M., D. W. Waugh, K. A. Boering, and R. A. Plumb (1999). Evaluation of transport in stratospheric models, *J. Geophys. Res.*, *104*, 18,815–18,839.

Hauck, M., Fritsch, F., Garny, H., and Engel, A. (2019). Deriving stratospheric age of air spectra using an idealized set of chemically active trace gases, *Atmos. Chem. Phys*., 19, 5269–5291, https://doi.org/10.5194/acp-19-5269-2019.

Hauck, M., Bönisch, H., Hoor, P., Keber, T., Ploeger, F., Schuck, T. J., and Engel, A. (2020). A convolution of observational and model data to estimate age of air spectra in the northern hemispheric lower stratosphere, *Atmos. Chem. Phys*., 20, 8763–8785, https://doi.org/10.5194/acp-20-8763-2020.

Johnson D. G., et al. (1999). Stratospheric age spectra derived from observations of water vapor and methane, *J. Geophys. Res., 104*, 21,595–21,602.

Kawatani, Y., Lee, J.N. and Hamilton, K. (2014). Interannual Variations of Stratospheric Water Vapor in MLS Observations and Climate Model Simulations. *Journal of the Atmospheric Sciences*, 71, 4072-4085, DOI: 10.1175/JAS-D-14-0164.1

Kida, H. (1983). General circulation of air parcels and transport characteristics derived from a hemispheric GCM, Part 2, Very long-term motions of air parcels in the troposphere and stratosphere, *J. Meteorol. Soc. Jpn.*, *61*, 510–522.

Konopka, P., Steinhorst, H.-M., Grooß, J.-U., Günther, G., Müller, R., Elkins, J. W., Jost, H.-J., Richard, E., Schmidt, U., Toon, G., and McKenna, D. S. (2004). Mixing and ozone loss in the 1999–2000 Arctic vortex: Simulations with the three-dimensional Chemical Lagrangian Model of the Stratosphere (CLaMS), J. Geophys. Res.-Atmos., 109, D02315, https://doi.org/10.1029/2003JD003792

Konopka, P., Tao, M., Ploeger, F., Hurst, D. F., Santee, M. L., Wright, J. S., & Riese, M. (2022). Stratospheric moistening after 2000. *Geophysical Research Letters*, *49*, e2021GL097609. https://doi.org/10.1029/2021GL097609

Li, F., Waugh, D. W., Douglass, A. R., Newman, P. A., Pawson, S., Stolarski, R. S., Strahan, S. E., and Nielsen, J. E. (2012). Seasonal variations of stratospheric age spectra in the Goddard Earth Observing System Chemistry Climate Model (GEOSCCM), *J. Geophys. Res.-Atmos*., 117, D05134, https://doi.org/10.1029/2011JD016877.

Livesey, N J, W G Read, P A Wagner, L Froidevaux, M L Santee, and M J Schwartz (2020). Version 5.0 x Level 2 and 3 Data Quality and Description Document (Tech. Rep. No. JPL D-105336 Rev. A). *Jet Propulsion Laboratory*.

Livesey, N. J., Read, W. G., Froidevaux, L., Lambert, A., Santee, M. L., Schwartz, M. J., Millán, L. F., Jarnot, R. F., Wagner, P. A., Hurst, D. F., Walker, K. A., Sheese, P. E., and Nedoluha, G. E. (2021). Investigation and amelioration of long-term instrumental drifts in water vapor and nitrous oxide measurements from the Aura Microwave Limb Sounder (MLS) and their implications for studies of variability and trends, Atmos. Chem. Phys., 21, 15409–15430, https://doi.org/10.5194/acp-21-15409-2021

Millán, L., Santee, M. L., Lambert, A., Livesey, N. J., Werner, F., Schwartz, M. J., et al. (2022). The Hunga Tonga-Hunga Ha'apai Hydration of the Stratosphere. *Geophysical Research Letters*, 49, e2022GL099381. https://doi.org/10.1029/2022GL099381

Mote, P.W., Rosenlof, K.H., Holton, J.R., Harwood, R.S. and Waters, J.W. (1996). An atmospheric tape recorder: The imprint of tropical tropopause temperatures on stratospheric water vapor. *Journal of Geophysical Research*, 101, 3989-4006.

Neu, J. L. and Plumb, R.A. (1999). Age of air in a 'leaky pipe' model of stratospheric transport. *Journal of Geophysical Research*, 104, D16, 19,243-19,255.

Niwano, M., Yamazaki, K. and Shiotani, M. (2003). Seasonal and QBO variations in ascent rate in the tropical lower stratosphere as inferred from UARS HALOE trace gas data. *Journal of Geophysical Research*, 108, 4794, doi:10.1029/2003JD003871

Peterson, D. A., Fromm, M. D., McRae, R. H. D., Campbell, J. R., Hyer, E. J., Taha, G., Camacho, C. P., Kablick, G. P., Schmidt, C. C., and DeLand, M. T. (2021). Australia's Black Summer pyrocumulonimbus super outbreak reveals potential for increasingly extreme stratospheric smoke events, Npj Clim. Atmos. Sci., 4, 38, https://doi.org/10.1038/s41612-021-00192-9

Ploeger, F. and Birner, T. (2016). Seasonal and inter-annual variability of lower stratospheric age of air spectra. *Atmospheric Chemistry and Physics*, 16, 10195-10213, doi:10.5194/acp-16-10195-2016

Ploeger, F., Legras, B., Charlesworth, E., Yan, X., Diallo, M., Konopka, P., Birner, T., Tao, M., Engel, A., and Riese, M. (2019). How robust are stratospheric age of air trends from different reanalyses? *Atmos. Chem. Phys*., 19, 6085–6105, https://doi.org/10.5194/acp-19-6085-2019.

Ploeger, F., Diallo, M., Charlesworth, E., Konopka, P., Legras, B., Laube, J. C., Grooß, J.-U., Günther, G., Engel, A., and Riese, M. (2021). The stratospheric Brewer–Dobson circulation inferred from age of air in the ERA5 reanalysis, *Atmos. Chem. Phys*., 21, 8393–8412, https://doi.org/10.5194/acp-21-8393-2021.

Podglajen, A. and Ploeger, F. (2019). Retrieving the age of air spectrum from tracers: principle and method, *Atmos. Chem. Phys.*, 19, 1767–1783, https://doi.org/10.5194/acp-19-1767-2019.

Pommrich, R., and coauthors (2014). Tropical troposphere to stratosphere transport of carbon monoxide and long-lived trace species in the Chemical Lagrangian Model of the

Stratosphere (CLaMS), Geosci. Model Dev., 7, 2895–2916, https://doi.org/10.5194/gmd-7-2895-2014

Randel, W., and Park, M. (2019). Diagnosing observed stratospheric water vapor relationships to the cold point tropical tropopause. *Journal of Geophysical Research: Atmospheres*, *124*. https://doi.org/10.1029/ 2019JD030648

Read, W. G., Lambert, A., Bacmeister, J., Cofield, R. E., Christensen, L. E., Cuddy, D. T., et al. (2007). Aura Microwave Limb Sounder upper tropospheric and lower stratospheric H_2O and relative humidity with respect to ice validation. *Journal of Geophysical Research*, *112*, D24S35. https://doi.org/10.1029/2007JD008752

Rieger, L. A., Randel, W. J., Bourassa, A. E., & Solomon, S. (2021). Stratospheric temperature and ozone anomalies associated with the 2020 Australian New Year fires. *Geophysical Research Letters*, *48*, e2021GL095898. https://doi.org/10.1029/2021GL095898

Schoeberl, M. R., A. R. Douglass, Z. Zhu, and S. Pawson (2003). A comparison of the lower stratospheric age spectra derived from a general circulation model and two data assimilation systems, J. Geophys. Res., 108(D3), 4113, doi:10.1029/2002JD002652.

Schoeberl, M. R., Douglass, A. R., Polansky, B., Boone, C., Walker, K. A., and Barnath, P. (2005). Estimation of stratospheric age spectrum from chemical tracers, *J. Geophys. Res*., 110, D21303, https://doi.org/10.1029/2005JD006125.

Tao, M., Konopka, P., Wright, J.S. *et al.* Multi-decadal variability controls short-term stratospheric water vapor trends. *Commun Earth Environ* **4**, 441 (2023). https://doi.org/10.1038/s43247-023-01094-9

Waugh, D. W. and Hall, T.M. (2002). Age of stratospheric air: Theory, observations, and models, *Reviews of Geophysics*, 40 (4), doi:10.1029/2000RG000101

Yu, P., Davis, S. M., Toon, O. B., Portmann, R. W., Bardeen, C. G., Barnes, J. E., et al. (2021). Persistent stratospheric warming due to 2019–2020 Australian wildfire smoke. *Geophysical Research Letters*, *48*, e2021GL092609. https://doi.org/10.1029/2021GL092609

Yu, W., Garcia, R., Yue, J., Russell, J. III, & Mlynczak, M. (2022).Variability of water vapor in the tropical middle atmosphere observed from satellites and interpreted using SD-WACCM simulations. *Journal of Geophysical Research: Atmospheres*, *127*, e2022JD036714. https://doi.org/10.1029/2022JD036714

Zhou, X., Dhomse, S. S., Feng, W., Mann, G., Heddell, S., Pumphrey, H., et al. (2024). Antarctic vortex dehydration in 2023 as a substantial removal pathway for Hunga Tonga-Hunga Ha'apai water vapor. *Geophysical Research Letters*, *51*, e2023GL107630. https://doi.org/10.1029/2023GL107630